2D-Sintering Kinetics of Two Model Fluids as Drops

Jean-Damien Muller,[†] Mosto Bousmina,[‡,§] and Abderrahim Maazouz*[,†,§]

LMM/IMP, UMR CNRS #5223, Université de Lyon, INSA de Lyon, Bâtiment Jules Verne, 69100 Villeurbanne, France, Canada Research Chair on Polymer Physics and Nanomaterials, Department of Chemical Engineering, CREPEC, Laval University, Sainte-Foy Québec, G1K 7P4 Québec, Canada, and Hassan II Academy of Science and Technology, Rabat, Morocco

Received October 23, 2007; Revised Manuscript Received January 8, 2008

ABSTRACT: The aim of the present work was to examine the effect of the rheological behavior of polymer liquids on the kinetics of the sintering process between two drops of the same liquid put in close vicinity of a solid surface. Nine samples of three different natures have been used: three poly(dimetylsiloxane)s (PDMS) of various viscosities, two polybutenes (PB) of different viscosities and four Boger fluids. The sintering experiments were carried out with a PTFE (polytetrafluoroethylene) substrate at room temperature. The surface tension of the samples was measured with the sessile drop method and the sintering process was captured by a CCD camera and the variation in time of the neck radius during was compared to Bellehumeur et al. model. The effects of viscosity, surface tension and relaxation time are discussed.

1. Introduction

When two drops of a liquid are brought into close contact, they coalesce, leading to a bigger drop. Coalescence may occur in emulsions with drop-matrix morphology during flow or at rest after cessation of flow. Such a process is very complex and involves the drainage of the thin film of the matrix entrapped in the gap between the two drops. Another simple coalescence process occurs during the sintering of two drops in a film-free state as illustrated in Figure 1. Such a situation can be generated by depositing two liquid drops in close vicinity on a solid substrate. Among the popular models for describing such film-free sintering process in Newtonian liquids was proposed by Frenkel:[1]

$$\frac{x}{r} = \left(\frac{3}{2}\frac{\gamma t}{\eta r}\right)^{0.5} \tag{1}$$

Here, x, r, t, γ, and η represent the neck radius, the initial particle radius, the time of sintering, the surface tension, and the viscosity of the liquid, respectively. Some refinements of the previous model were given by Eshelby.[2] The approach was then extended to account for the viscoelastic effects. A simple modification of Frenkel model was proposed by Lontz[3] who introduced a simple relaxation process involving one relaxation time:

$$\frac{x}{r} = \left(\frac{3}{2}\frac{\gamma t}{\eta r}\right)^{0.5} \frac{1}{1 - e^{(-t/\lambda)}} \tag{2}$$

Pokluda et al.[4] modified the model by taking into account the change in particle radius during the coalescence process. Coalescence in liquids obeying convected Maxwell model was proposed by Bellehumeur et al.[5] Under the quasi-steady state approximation, the Bellehumeur et al. model may be written as follows:

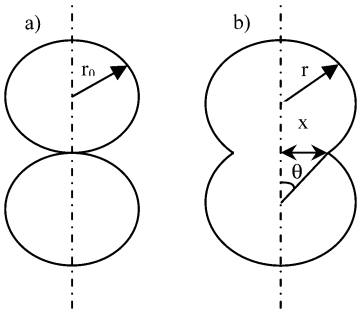

Figure 1. Geometrical illustration of the sintering process of two drops at (a) $t = 0$ s and (b) $t > 0$ s. The parameters r, x, and θ represent the radius, the neck radius, and the sintering angle, respectively.

$$8(\beta\lambda K_1\theta')^2 + \left(2\beta\lambda K_1 + \frac{\eta_0 r_0}{\gamma}\frac{K_1^2}{K_2}\right)\theta' - 1 = 0 \tag{3}$$

Here η_0 is the zero-shear viscosity and r_0 the uniform initial radius of the drops. K_1 and K_2 are geometrical parameters given by

$$K_1 = \frac{\sin\theta}{(1+\cos\theta)(2-\cos\theta)} \tag{4}$$

$$K_2 = \frac{2^{-5/3}\cos\theta\sin\theta}{(1+\cos\theta)^{4/3}(2-\cos\theta)^{5/3}} \tag{5}$$

θ is designed as the sintering angle as illustrated on Figure 1. β is the Maxwell coefficient that takes the value $+1$ for the upper convected Maxwell model (UCM).

It was found that the steady-state UCM model does not describe well the sintering process of all viscoelastic materials. An effort was thus made to develop a model in which the transient rheology was taken into account.[6,7] It was concluded that the influence of viscoelasticity was limited to the first step of the coalescence process. For long times, the transient model converges to the Newtonian solution. This can be explained by the following three steps: (1) at short time, the behavior is

* Corresponding author. Telephone: +33 4 72 43 63 32. Fax : +33 4 72 43 85 15. E-mail address: abderrahim.maazouz@insa-lyon.fr.
† LMM/IMP, UMR CNRS #5223, Université de Lyon, INSA de Lyon.
‡ Canada Research Chair on Polymer Physics and Nanomaterials, Department of Chemical Engineering, CREPEC, Laval University.
§ Hassan II Academy of Science and Technology.

10.1021/ma702349s CCC: $40.75
Published on Web 02/22/2008

dominated by an elastic adhesive contact, (2) at intermediate time, there is a zipping contact growth, and (3) in the later stage, the drops undergo a stretching contact process. The variation of the neck radius during the three steps was found to be described by a scaling law as a function of material properties or time.[8] During the first step, the drops undergo deformation and create a finite contact surface. The dimensionless neck radius is proportional to material properties with a power index equal to $^1/_3$.[9,10] The second step is accommodated by viscous deformation, where growth of the neck radius experiences a competition between the adhesive intersurface forces and the viscoelastic deformation. During this step x/r evolves proportionally to $t^{1/7}$ for simple Maxwell viscoelastic materials.[11] In the later stage for $t > t_{viscous}$, the liquid behaves in a Newtonian fashion and the neck radius becomes proportional to $t^{1/2}$ as predicted by Frenkel model.[12,13] $t_{viscous}$ can be defined by

$$t_{viscous} = \frac{1}{16}\left(\frac{63\pi^3}{2}\right)^{2/5}\frac{r}{C_1 W}\left(\frac{\delta_c}{r}\right)^{4/5} \quad (6)$$

C_1 is a material constant, W represents the cohesive forces and δ_c is a critical separation below which the adhesive force is constant.

Mazur and Plazek[14] made the assumption that the coalescence can be viewed as the sum of the elastic adhesive contact and the Newtonian contributions, but the predicted coalescence kinetics are too fast. Lin et al.[15] modeled the sintering process as the succession of these 3 contributions and obtained better results.

As described above, intensive efforts have been devoted to the modeling of the coalescence process. Efforts have also been made to experimentally verify the predictions of such models for polymeric systems.[16] The studied materials were polymers of various families (e.g., PMMA, polyethylenes, polypropylenes, copolymers, EBA, EVA, polycarbonates, PVC, etc.). Using these types of polymers presents certain difficulties. First, the polymers must be heated, and in most cases, an inert gas must be used to avoid thermal degradation. Second, the melting of the polymer does not occur instantaneously. This can give rise to a gradient of temperature between the melted surfaces that start to undergo sintering and the bulk that has a lower temperature. This may be source of important errors mainly for the first step at short times of the sintering process. Third, in most cases, polymeric powders or particles with non-spherical shapes are used for the experiments. This is a major disadvantage for the accuracy of the experiments (effect of anisotropy) and for the comparison of the experimental data with the models. Image analysis can provide an equivalent radius for non-spherical particles, but it would be better to use drops with rather spherical initial shape. Fourth, when dealing with "classical" polymers, it is difficult to separate the elastic and the viscous contributions during sintering. Additionally, commercial polymers usually contain additives such as stabilizers and lubricants. These small molecules additives migrate to the surface and change the surface tension and therefore the whole process of sintering.

To overcome the above difficulties, the present work deals with the study of the sintering process kinetics using well characterized model liquids. Both Newtonian liquids (liquids with constant viscosity and zero elasticity) such as poly(dimethylsiloxane) (PDMS) and polybutenes (PB), and Boger fluids (liquids with constant viscosity but with nonzero elasticity) are used. The obtained results are compared to Bellehumeur et al. model. We chose this model because it pretty well describes sintering kinetics and it can be easily included in a global program to describe an entire processing cycle. Moreover, the physical parameters necessary for this model can be measured simply by only 2 experiments.

Table 1. Zero-Shear Viscosity at 25° of the 3 PDMS and the 2 PBs

sample	zero-shear viscosity (Pa·s) at 25 °C
PDMS1	10.6
PDMS2	28.9
PDMS3	80.8
PB1	23
PB2	502

Table 2. Composition of the Various Prepared Boger Fluids

sample	% kerosene (solvent)	% polyisobutylene (polymer)	% polybutene (polymer solvent)
BF1	6.98	0.22	92.8 (PB1)
BF2	6.2	0.8	93 (PB1)
BF3	6.98	0.22	92.8 (PB2)
BF4	6.2	0.8	93 (PB2)

2. Experimental Section: Materials and Methods

2.1. Simple Fluids. Three PDMS and two PB samples of different viscosities were chosen for the present study. Table 1 presents the nomenclature of the various samples with their zero-shear viscosities measured at 25 °C. Their complete rheological properties are discussed in part 2.

2.2. Boger Fluids Formulation. The Boger fluids were obtained using PB as the polymer matrix, kerosene as the solvent and polyisobutylene (PIB) as the minor phase. Two PBs were used in order to investigate the effect of viscosity. According to the supplier, the average weight molecular weight, M_w, of PB1 is 920 g/mol, and that PB2 is 2300 g/mol.

In order to obtain an efficient mixing of the components, PIB was first added to kerosene and then the solution was submitted to mixing during about 48 h to obtain a homogeneous mixture to which PB was added afterward. The three components mixture was gain agitated with a stirrer blade for 2 weeks at 50 °C. After mixing, the solution was placed in a vacuum drying oven at 70 °C for 4 weeks to eliminate the eventual traces of kerosene. The composition of the prepared four Boger fluids is given in Table 2.

2.3. Surface Tension Measurements. The surface tension of the liquids was measured at 25 °C with the sessile drop method. Three different substrates of which at least one was nonpolar, were used. The substrates used were PTFE, aluminum, and glass. One drop of the liquid, as small as possible, was deposited on the substrate and was left for a time period ranging from 1 and 12 h in order to reach equilibrium. Its profile was then recorded using a CCD camera. The contact angle, α, between the drop and the substrate was measured and the surface tension was evaluated using image analyses software.

2.4. Rheological Tests. Small amplitude oscillatory shear tests were carried out with a stress-controlled rotational rheometer AR1000 from TA Instruments, with a cone and plate geometry (diameter = 60 mm, angle = 2° ≈ 0.035 rad, gap = 66 μm). The frequency was ranged from 5×10^{-3} to 7×10^2 rad/s. All rheological measurements were carried out in the linear viscoelastic regime as was verified by preliminary strain sweep tests. The frequency sweep experiments were carried out at various temperatures ranging from 25 to 65 °C by a step of 10 °C. The various isotherms were then superimposed on a single master curve at 25 °C using time−temperature superposition procedure.

2.5. Sintering Experiments. The sintering experiments were conducted on a regulated hot stage on which the drops were deposited. Zeiss binoculars and a Pantera CCD digital camera were linked to a computer, which allowed the recording of the images at regular intervals. All experiments were carried out at 25 °C. The fluids were colored with a silicon carbide SiC powder in order to increase the contrast between the drops and the substrate. The amount of SiC in each fluid was approximately 1 wt %, and the

size of the drops was about 5 μm. It was verified experimentally that the addition of SiC did not modify neither the rheological properties of the matrixes nor their surface tension. Because of their relatively low viscosities, the drops adopt more or less instantaneously a spherical shape. The entire process of sintering was then recorded. At short times, i.e., when the neck radius grows quickly, all images were analyzed. Intervals between each image ranged from 0.22 to 1.5 s. When the sintering rate decreased, only one image was considered every 5 or 10 images. Each coalescence experiment was repeated three times, and the estimated incertitude was approximately 4%.

3. Material Characterization

3.1. Surface Tension Measurements. Surface tension was evaluated for the all used samples. The contact angles between the liquids and three substrates were measured to determine the polar, γ_L^p, and the dispersive, γ_L^d, components of the liquid surface tension. When considering a liquid drop of surface tension γ_L on a solid substrate of surface tension γ_S (see Figure 2), the equilibrium at the triple point can be written as

$$\gamma_S = \gamma_{SL} + \gamma_L \cos \alpha \tag{7}$$

γ_{SL} is the interfacial tension between the liquid and the substrate and α the contact angle. According to Owens and Wendt,[17] γ_{SL} can be expressed as

$$\gamma_{SL} = \gamma_S + \gamma_L - 2(\gamma_S^d \gamma_L^d)^{1/2} - 2(\gamma_S^p \gamma_L^p)^{1/2} \tag{8}$$

According to eqs 7 and 8, this leads to

$$\gamma_L(1 + \cos \alpha) = 2(\gamma_S^d \gamma_L^d)^{1/2} + 2(\gamma_S^p \gamma_L^p)^{1/2} \tag{9}$$

In the above equation, the values of γ_S^d, γ_S^p, and α are known for each used substrate. Since γ_S^d is not equal to zero, one can write:

$$\frac{(1 + \cos \alpha)}{2\sqrt{\gamma_S^d}} = \frac{1}{\gamma_L}\sqrt{\gamma_L^p}\sqrt{\frac{\gamma_S^p}{\gamma_S^d}} + \frac{1}{\gamma_L}\sqrt{\gamma_L^d} \tag{10}$$

This is a linear equation, in which the slope and the intercept points are respectively:

$$A = \frac{1}{\gamma_L}\sqrt{\gamma_L^p} \tag{11}$$

$$B = \frac{1}{\gamma_L}\sqrt{\gamma_L^d} \tag{12}$$

By remembering that $\gamma = \gamma^p + \gamma^d$, and combining eqs 11 and 12, the expressions of γ_L^p and γ_L^d are given by

$$\gamma_L^p = \frac{A^2}{(A^2 + B^2)^2} \tag{13}$$

$$\gamma_L^d = \frac{B^2}{(A^2 + B^2)^2} \tag{14}$$

By plotting

$$\frac{(1 + \cos \alpha_i)}{2\sqrt{\gamma_{S_i}^d}} = f\left(\sqrt{\frac{\gamma_{S_i}^p}{\gamma_{S_i}^d}}\right) \tag{15}$$

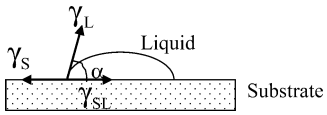

Figure 2. Equilibrium of a liquid drop on a substrate. γ_L, γ_S and γ_{SL} represent the surface tension of the liquid, the surface tension of the substrate and the interfacial tension between the liquid and the substrate, respectively.

where i is the number of the substrate and the polar and the dispersive components of the liquid can be easily determined from the above expressions. This method has the advantage of being relatively simple, but its main disadvantage is its poor accuracy due mainly to the roughness of the substrate surface. The obtained results are given with an average error of ± 0.2 mN/m.

Table 3 presents the surface tension results for all tested samples. It is found that the polar components are weak as compared to their dispersive counterparts, and for all samples, the polar components could be considered as negligible. This means that measurements could be performed with only one nonpolar substrate like PTFE. The results of the surface tension calculated when using PTFE as substrate are also given in Table 3. These values were subsequently used to calculate the theoretical sintering rates, as will be presented in part IV.

The surface tension values for the three PDMS samples are quite similar, whereas the two PBs are characterized by different surface tensions. The surface tension of PB1 is 26.3 mN/m, whereas that of PB2 is 27.4 mN/m. The surface tension of the Boger fluids has a value quite equal to that of their respective matrixes: BF1 and BF2 are characterized by a surface tension having a value quite similar to that of their matrix (PB1) and that of BF3 and BF4 quite identical to that of their matrix (PB2).

3.2. Rheological Characteristics. 3.2.1. PDMS and PB Samples. Figures 3 and 4 report the complex shear viscosity as a function of frequency for PDMS and PB samples. All samples present a large Newtonian plateau followed by a small decrease in viscosity at high frequencies mainly for large molecular weight samples. However up to 80 rad/s, all the samples behave as Newtonian liquids. Beyond this value PDMS3 and PB2 show a decrease in viscosity as a function of frequency (frequency-thinning behavior).

3.2.2. Boger Fluids. Figures 5 and 6 show the variation of the storage shear modulus and the complex shear viscosity as a function of frequency for BF1, BF2 and BF3, BF4, respectively. The two sets of samples differ in the nature of PB used as a matrix (see Table 2). BF1 and BF2 have the same matrix (PB1) and differ only in the concentration of PIB. BF3 and BF4 have the matrix PB2 and differ also by the concentration of their PIB minor phase. BF1 and BF2 samples exhibit quite the same behavior as a function of frequency with a clear Newtonian plateau in the low-frequency region (viscosity is constant and G' is almost zero) with a zero-shear viscosity of about 17 Pa·s for BF1 and of about 30 Pa·s for BF2, followed by a sharp decrease in viscosity before reaching a second plateau at high frequencies. Such a decrease starts at approximately 0.2 rad/s and extends to 50 rad/s. G' and G'' are also quite parallel (gel-like behavior) over the whole frequency range. It is also worth to note that a small change in the concentration of PIB (from 0.22% to 0.8%) induces an important variation in the magnitude of the storage modulus and viscosity.

The second series (BF3 and BF4) shows a completely different trend with a Newtonian viscosity in the low-frequency region followed by a smooth transition toward a second plateau for intermediate frequencies. The value of the viscosity of the

Table 3. Surface Tension Values for All Samples Obtained with Three Substrates (Columns 2−4) as Well as Merely One Nonpolar Substrate (Column 6)[a]

	measurements with three substrates: PTFE. aluminum and glass at 25 °C				
sample	γ_L^p (mN/m)	γ_L^d (mN/m)	γ_L (mN/m)	% contribution of polar part γ_L^p/γ_L	measurements with only PTFE at 25 °C $\gamma_L^d = \gamma_L$ (mN/m)
PDMS1	0.6	22.4	23.0	2.8	23.3
PDMS2	0.5	23.1	23.6	2.3	23.8
PDMS3	0.6	22.7	23.3	2.6	23.6
PB1	0.3	26.1	26.4	1.1	26.3
PB2	0.2	27.6	27.8	0.7	27.4
BF1	0.2	26.3	26.5	0.8	26.5
BF2	0.4	26.1	26.5	1.5	26.3
BF3	0.2	27.3	27.5	0.7	27.2
BF4	0.3	27.3	27.6	0.9	27.3

[a] The contribution of the polar component to the surface tension is displayed in column 5.

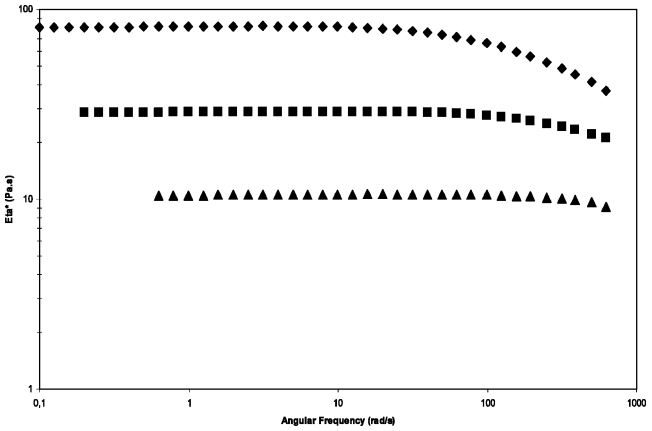

Figure 3. Complex shear viscosity vs frequency for PDMS1 (▲), PDMS2 (■), and PDMS3 (◆) at 25 °C.

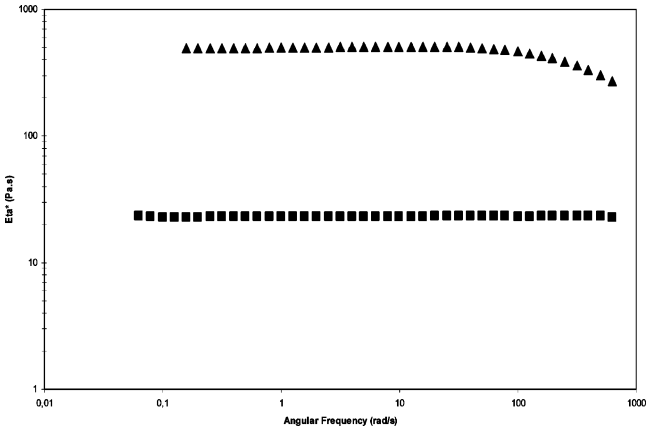

Figure 4. Complex shear viscosity vs frequency for PB1 (■) and PB2 (▲) at 25 °C.

second plateau is only slightly smaller than the value of the first Newtonian plateau. At approximately 70 rad/s, the viscosity shows a second transition with a decrease in viscosity with frequency. The difference in behavior of the two series is due to the difference in the behavior of their polymer matrix. In fact, in comparison with Figure 3, the high frequency-thinning behavior (similar to shear-thinning) observed in BF3 and BF4 can be linked with that of PB2. In contrast, PB1 did not show any frequency-thinning above 20 rad/s (Figure 4) and therefore the corresponding Boger fluids, BF1 and BF2 show a second plateau at high frequencies.

The two transitions appearing in the series BF3, BF4 is also reflected on G' that shows a small pseudoplateau before reaching

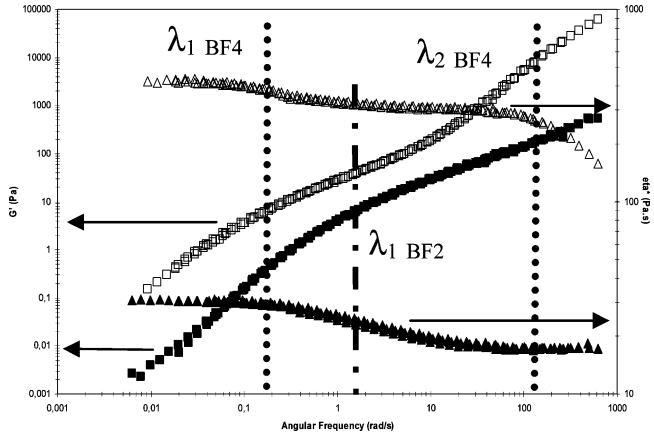

Figure 5. Rheological behavior of BF2 (▲, ■) and BF4 (△, □). The elastic modulus (■, □) is reported on the left axis, whereas the complex viscosity is displayed on the right axis (▲, △).

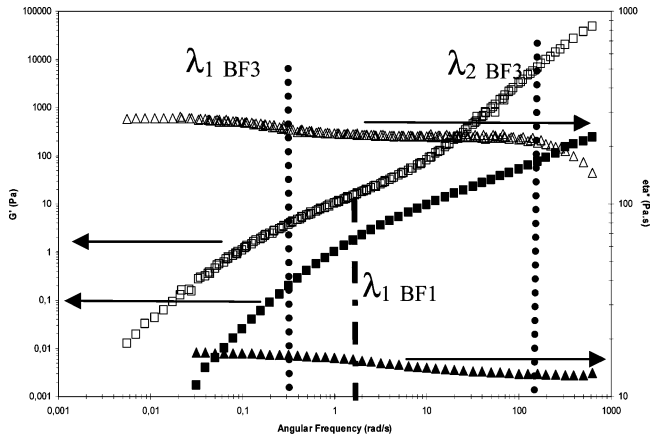

Figure 6. Rheological behavior of BF1 (▲, ■) and BF3 (△, □). The elastic modulus (■, □) is reported on the left axis, whereas the complex viscosity is displayed on the right axis (▲, △).

the terminal-zone, where it decreases linearly with lowering of frequency with a slope of 2 in log−log scale. The first decrease in viscosity is mainly due to the presence of PIB, whereas the second corresponds to PB contribution. Such a transition can also be reflected by weight-average characteristic relaxation time.

Characteristic relaxation times were determined from the Cole−Cole diagram (Figures 7 and 8) that shows a single maximum for BF1, BF2 (a single characteristic relaxation time) and two maxima for BF3 and BF4 (two relaxation times corresponding to $\lambda_i\omega_i = 1$, where $i = 1,2$). The results are

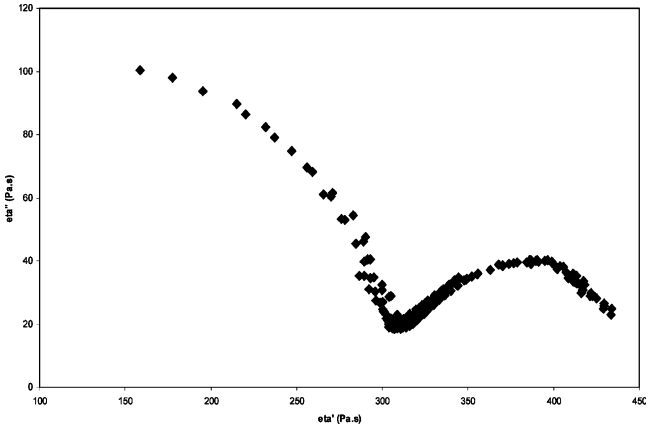

Figure 7. Cole−Cole diagram for BF4.

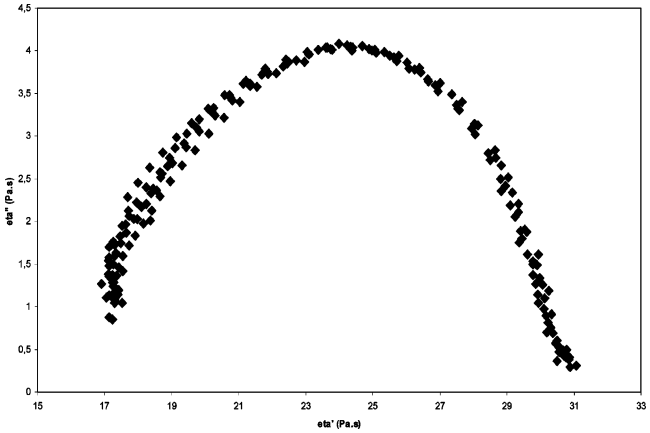

Figure 8. Cole−Cole diagram for BF2.

Table 4. Rheological Characteristics for PDMS and PB Samples, Where the Relaxation Times Were Calculated with the Cole−Cole Method and with the Fitting Method Using the Maxwell Model

		λ (s)	
fluid	η_0 (Pa·s)	Cole−Cole method	fitting method
PDMS1	10.6	1.5×10^{-4}	5.7×10^{-4}
PDMS2	28.9	1.5×10^{-3}	1.5×10^{-3}
PDMS3	80.8	3.1×10^{-3}	5.4×10^{-3}
PB1	23	10^{-5}	6.3×10^{-5}
PB2	502	2.6×10^{-3}	3.1×10^{-3}

Table 5. Zero-Shear Viscosities and Relaxation Times for the Boger Fluids (Columns 2, 3, and 4)[a]

fluid	η_0 (Pa·s)	λ_1 (s)	λ_2 (s)	λ_{PB} (s)
BF1	17	0.6	3.6×10^{-5} [b]	10^{-5}
BF2	30.8	0.9	10^{-4} [b]	
BF3	275	3.6	4×10^{-3}	2.6×10^{-3}
BF4	420	5.3	10^{-2}	

[a] The relaxation times for PB used in each Boger fluid are recalled in column 5. Relaxation time was determined by the Cole−Cole method, except as shown. [b]Relaxation time that was estimated by a numerical simulation.

presented in Table 5. It is observed that the relaxation time λ_1 is strongly dependent on PIB concentration, as it increases from 3.6 s for BF3, to 5.3 s for BF4, which has the higher PIB concentration. λ_2 is slightly higher than λ_{PB}, but the values are in the same order of magnitude. This effect may be due to PIB, as an increase in PIB would also lead to an increase in λ_2.

The viscosity of the Boger fluids is also dependent on PIB concentration. It increases from 17 Pa·s for BF1 to 30.8 Pa·s for BF2. Similarly, an equivalent trend is for BF3 and BF4.

Besides the main characteristic relaxation times, the Boger fluids are characterized by a spectrum of relaxation times. Boger fluids were supposed to have a constant viscosity on the whole frequency range. However, the fluids used in the present work are characterized by a frequency dependent viscosity. The rheological behavior of BF samples is rather described by a spectrum of relaxation times corresponding to various types of viscoelastic relaxation.

The experimental dynamic moduli of Boger fluids were fitted with a generalized Maxwell model using

$$G'(\omega_i) = \sum_{k=1}^{N} \frac{\eta_k \lambda_k \omega_i^2}{1 + (\omega_i \lambda_k)^2} \tag{16}$$

$$G''(\omega_i) = \sum_{k=1}^{N} \frac{\eta_k \omega_i}{1 + (\omega_i \lambda_k)^2} \tag{17}$$

Here, ω_i is the frequency of the ith data point. The fitting parameters were obtained by minimizing the sum of the squared difference between the predicted and the experimental moduli. In the present case, the samples are mixtures of PB characterized by short chains and PIB characterized by long chains (high molecular weight). Therefore, four to six modes were necessary to obtain a good fit of the dynamic moduli of the Boger fluids. Table 6 gives the determined λ_i,η_i parameters of the four to six modes for the four Boger fluids.

With these data, three families of relaxation times could be considered. The first includes the short times (10^{-5}−10^{-4} s), corresponding to the PB contribution (relaxation time of PB lies within 10^{-5}−10^{-3} s). The second corresponds to long times (>1 s) and could be attributed to long chains of PIB. Finally, the intermediate times (10^{-2}−10^{-1} s) are due to entanglements of PIB and PB chains.

Sintering Experiments. All sintering experiments were conducted on a PTFE substrate. Figure 9 shows the typical shape evolution in time of two PDMS1 drops put in close vicinity. Initially, the two drops had a nice and regular hemispherical shape and then undergo sintering process in a regular fashion with a clear change in the contact region and the neck radius. As stated in the introduction, this system offers more experimental accuracy in comparison with commercial high molecular weight thermoplastic polymers that show irregular shapes and nonisothermal and degradation problems.

The observed evolution in shape during sintering was then compared to Bellehumeur et al. model using the parameters obtained from the rheological tests (η_0, λ), the surface tension measurements (γ) and the initial drop radius (r_0). The evolution of x/r as a function of time was obtained by integrating eq 2 using Runge−Kutta routine. It should be noted that it was impossible to measure the initial value of x/r. Therefore, the first x/r value obtained experimentally was taken as the initial value in the integration and in the worst case this value ranged between 0.25 and 0.35.

Table 7 gives the viscous time t_v for each fluid as indicated by eq 6. Beyond this time, the flow is only viscous. The low values of t_v confirm that the use of Bellehumeur's model is sufficient. For comparison purposes, the experimental data can also be fitted by the following simple expression:

$$\frac{x}{r} = 1 - K\mathrm{e}^{-(t/\tau)} \tag{18}$$

From this fitting, a characteristic time τ and the slope $\mathrm{d}(x/r)/\mathrm{d}t$ at the initial stage can be deduced. Figures 10, 11, and 12 show the results for PDMS, polybutenes, and the Boger fluid samples,

Table 6. Relaxation Spectra for the Boger Fluids

	BF1		BF2		BF3		BF4	
mode	λ_k (s)	η_k (Pa·s)	λ_k (s)	η_k (Pa·s)	λ_k (s)	η_k (Pa·s)	λ_k (s)	η_k (Pa·s)
1	3.6×10^{-5}	6.69	10^{-4}	17.5	2.3×10^{-5}	149.7	3.7×10^{-4}	170.8
2	2.3×10^{-4}	6.74	9×10^{-2}	5.70	3.1×10^{-3}	72.8	2.5×10^{-3}	123.2
3	1.6×10^{-2}	1.22	1.5	7.01	1.3×10^{-1}	14.6	2.2×10^{-1}	35.9
4	1.9×10^{-1}	9.4×10^{-1}	32.4	4.8×10^{-1}	4.3	24.3	3.8	60.9
5	6.6×10^{-1}	1.38			38.0	5.1	33.9	28.2
6	4.3	6.6×10^{-2}						

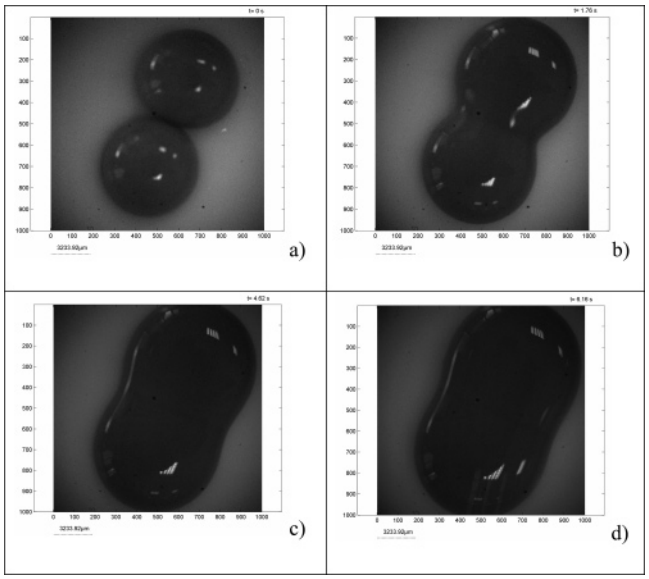

Figure 9. Sintering of PDMS1 at (a) $t = 0$ s; (b) = 1.76 s; (c) $t =$ 4.62 s; (d) $t = 6.16$ s.

Table 7. Viscous Time Given by Eq 6 for All the Nine Fluids[a]

fluid	t_v (s)
PDMS1	4.7×10^{-3}
PDMS2	1.2×10^{-2}
PDMS3	3.5×10^{-2}
PB1	8.9×10^{-3}
PB2	1.9×10^{-2}
BF1	6.7×10^{-3}
BF2	1.2×10^{-2}
BF3	1.0×10^{-2}
BF4	1.6×10^{-2}

[a] In a first approximation, we can consider that $C_1 = 4/\eta_0$ and $W = 2\gamma$. In order to maximize the results, we have chosen $\delta_c = 1$ μm.

respectively. The figures also include Bellehumeur et al. model. The parameters used were the viscosities, surface tensions, relaxation times, and initial radii. For all fluids, r_0 varied between 3.9 and 4.2 mm. The fitting parameter τ in eq 18 is given in Table 8, as well as the time required to reach 99% of completion, i.e., t_{99}, and the initial slope.

3.3.1. Effect of the Viscosity. The effect of viscosity on the sintering kinetics of PDMS samples is shown in Figure 10. PDMS1 displays a faster sintering than PDMS2 and PDMS3. From Table 8, it becomes evident that this can be quantitatively confirmed by t_{99}. PDMS1 needs 6.2 s to undergo sintering, while 14.7 and 42.3 s are necessary for PDMS2 and PDMS3. The first step of the sintering process is governed by diffusion at the interface between the two drops put in close vicinity. Once the initial barrier energy is overcome, the two drops start to coalesce due to self-diffusion of the polymeric chains on both sides of the interface. Self-diffusion coefficient in polymer networks scales as the inverse of viscosity, $D \sim 1/\eta^{\nu}$, where the exponent ν is close to $^2/_3$. The time of diffusion over a distance L scales as the inverse of the diffusion coefficient, $t =$

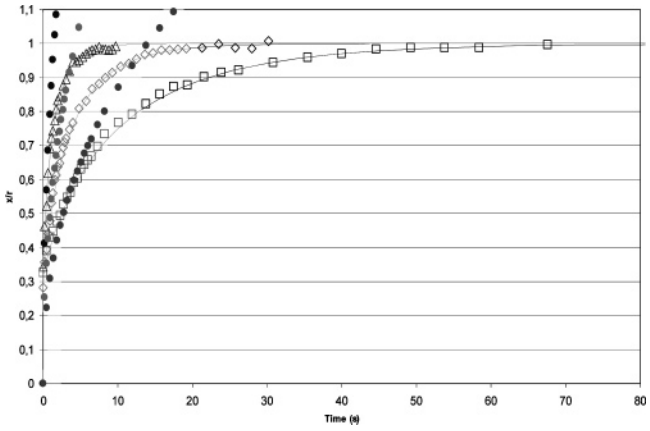

Figure 10. Coalescence curves for PDMS1 (△), PDMS2 (◇), and PDMS3 (□). The solid lines represent the Bellehumeur et al. model for each PDMS material and the full circles are Frenkel's model.

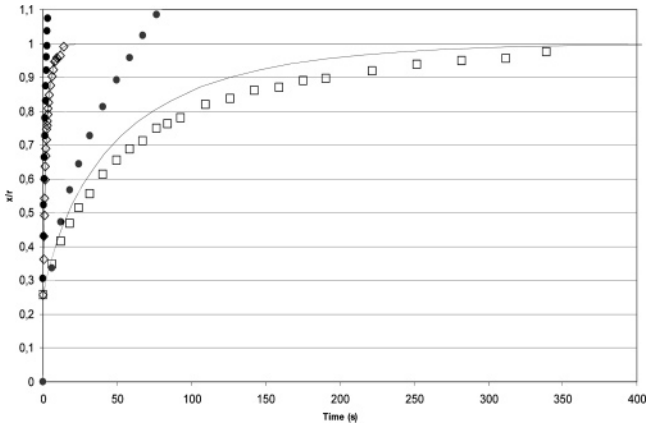

Figure 11. Coalescence curves for PB1 (◇) and PB2 (□).The solid lines represent the Bellehumeur et al. model for each polybutene material (overlapped for PB1). The full circles are Frenkel's model.

L^2/D, and therefore it increases proportionally to the viscosity $t \sim \eta^{\nu}$. For instance, PDMS3 is approximately 2.8 times more viscous than PDMS2. The diffusion time in the two samples should scale in the same proportion with a powerν. An indirect way to confirm such proportionality is to compare the viscosity ratio η(PDMS3)/η(PDMS2) with the ratio of experimental characteristic times τ(PDMS3)/τ(PDMS2) or t_{99}(PDMS3)/t_{99}-(PDMS2). Such a ratio is 2.78 for τ and 2.87 for t_{99}. The same proportionality is also reasonably confirmed for PDMS2/PDMS1 and PDMS3/PDMS1.

The initial slope also provides an indication on the sintering rate. It is of about 0.439 s^{-1} for PDMS1 and decreases to about 0.070 s^{-1} for PDMS3. Again the ratio between the sintering rates scales approximately is the same manner as the inverse of the viscosity ratio. Such a sintering rate was also found to be approximately given by the ratio $\gamma/\eta r_0$ as it is reported in Table 8.

Figure 10 reports also the comparison between the experimental and Bellehumeur et al. model predictions. The results

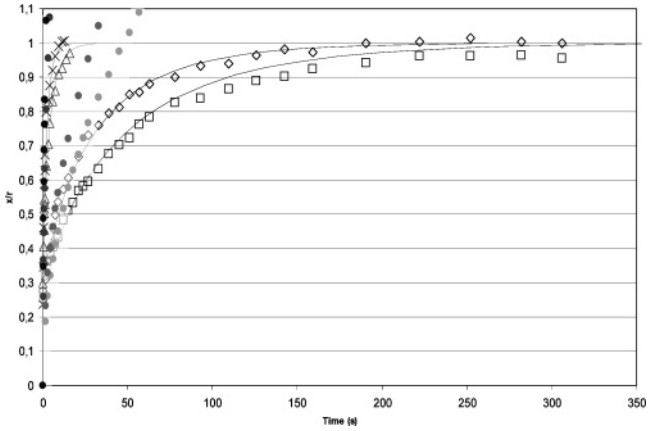

Figure 12. Coalescence curves for the Boger fluids. BF1 and BF2 are represented by symbols × and △ respectively. Data for BF3 (◇) and BF4 (□) are also plotted. The solid lines represent the Bellehumeur et al. model for each Boger fluid (overlapped for BF1 and BF2). Frenkel's model is plotted with full circles.

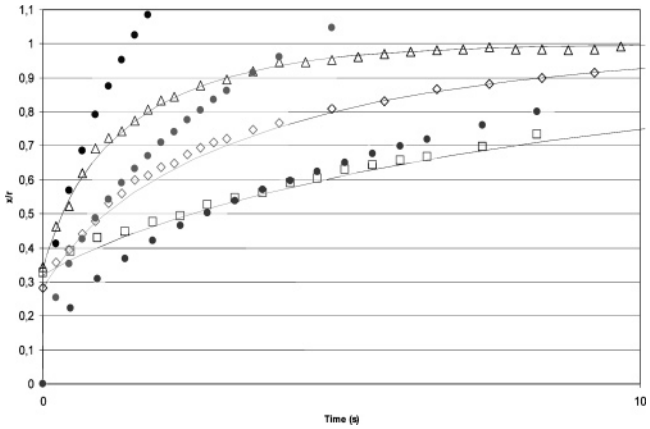

Figure 13. Detail of Figure 10 for the early stages of the sintering of PDMS.

Table 8. Fitting Parameters for the Empirical Model. Column 1 Gives the Initial Slope[a]

fluid	$d(x/r)/dt\|_{t\to 0}$ (s^{-1})	$\gamma/\eta r_0$	τ (s)	t_{99} (s)
PDMS1	0.439	0.508	1.49	6.2
PDMS2	0.208	0.206	3.45	14.7
PDMS3	0.070	0.073	9.61	42.3
PB1	0.339	0.271	2.19	9.5
PB2	0.010	0.013	74.62	322.5
BF1	0.456	0.378	1.68	7.3
BF2	0.200	0.204	3.50	14.9
BF3	0.023	0.024	30.49	130.5
BF4	0.014	0.015	52.63	225.0

[a] Column 2 is the scaling time time. Column 3 is the characteristic time (see eq 17). t_{99} represents the time necessary to reach 99% of completion. The last column gives the values for the reduced time (eq 18).

show that the model captures nicely the whole sintering kinetics for the three PDMS samples. A close zoom on the figures (Figures 13−15) reveals only slight differences that lie within experimental errors.

3.3.2. Effect of the Viscosity and Interfacial Tension. PB samples display a sintering kinetics similar to that of PDMS and depend quite in the same fashion on viscosity. PB1, which has a low viscosity and a Newtonian behavior, exhibits a faster sintering process (t_{99} = 9.46 s) than PB2 (322.5 s). The comparison between the experimental data and the theoretical predictions shows that the model overestimates the radius neck

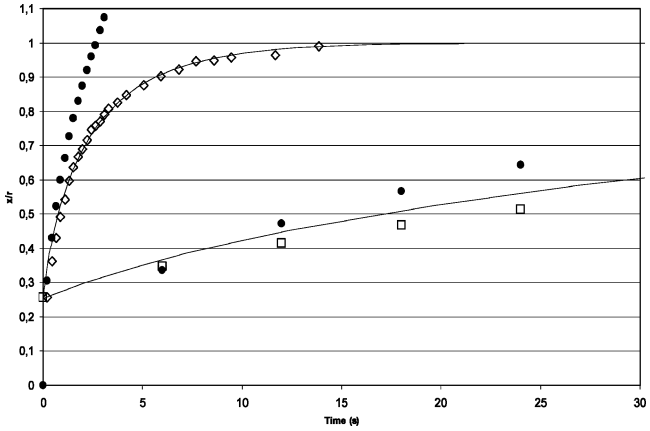

Figure 14. Detail of Figure 11 for the beginning of the sintering of PBs.

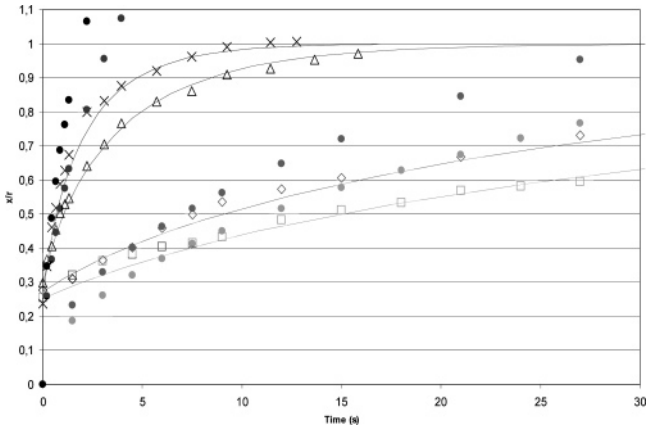

Figure 15. Detail of Figure 12 for the very start of sintering of FBs.

Table 9. Values of Interfacial Tension on a Substrate of PTFE as Well as the Spreading Coefficient PDMS, PB, and Boger Fluids

fluid	interfacial tension with PTFE (mN/m)	spreading parameter on PTFE (mN/m)
PDMS1	8×10^{-3}	−0.84
PDMS2	1.9×10^{-2}	−1.34
PDMS3	1.2×10^{-2}	−1.06
PB1	0.14	−3.91
PB2	0.24	−5.12
BF1	0.16	−4.12
BF2	0.15	−3.94
BF3	0.23	−4.95
BF4	0.24	−5.09

for PB2 over quite the whole time scale of the sintering process. A part from the frequency-thinning behavior that characterizes PB2, the discrepancy between the model predictions and experimental data might be attributed to the effect of interfacial tension. In fact, PTFE substrate has a surface tension γ_s of about 22.5 mN/ m, whereas that of PB2 is of about γ_l = 27.4 mN/m. The interfacial tension deduced from eq 5 is approximately γ_{sl} = 0.24 mN/m. The spreading parameter S of the PB2 on the surface of PTFE can be estimated by

$$S = \gamma_S - (\gamma_L + \gamma_{SL}) \tag{19}$$

Table 9 gives the interfacial tension and the spreading coefficient for all fluids. If $S > 0$, the wetting is favorable and the liquid wets well the substrate. On the other hand, if $S < 0$, the wetting is partial, and the liquid remains as a drop. For PB2, $S = -5.12$ mN/m, which reveals that it has a tendency not to wet the

substrate. A good sintering requires as a first requirement a good spreading of the liquid on the surface. If the liquid does not spread, the diffusion at the interface and thus the sintering process should overcome the additional barrier energy due to surface tension that tend to maintain the drops in their initial spherical shape.

Negative spreading parameters are also obtained for PDMS and PB1. However, Bellehumeur et al. model fits reasonably well the experimental data for these samples. For PDMS samples, the spreading parameters are higher than those of PB samples. Consequently, PDMS should spread better on PTFE than PB, explaining the agreement between the model predictions and the experimental results.

As was observed, the model fits also well the sintering data for PB1 despite a low spreading parameter. One possible explanation is that the first stage of the sintering process is governed by two contributions: (i) the wetting capacity and (ii) diffusion at the interface. Diffusion in highly viscous liquids is very slow and this may slow down the sintering process, although the liquid might have some affinity with the surface and wets it well. From the other side, a low viscosity liquid is characterized by a favorable diffusion coefficient. Such a favorable effect can be retarded by its small wetting capacity on the surface of the substrate. Clearly, conversely to emulsions, where the coalescence process may be seen as a three-dimensional process that can occur in all directions, sintering of two droplets deposited in close vicinity on a substrate is a two-dimensional process governed by two additional parameters related to the surface of the substrate: (i) the thermodynamic wetting energy and (ii) the mechanical wetting energy (roughness) that favors the initial step of sintering. Such parameters are not considered in any theoretical model.

3.3.3. Effect of the Relaxation Time. Figure 12 illustrates the sintering of the Boger fluids. BF1 and BF2 were found to coalesce much faster than BF3 and BF4. This can be explained by the large differences in viscosity between the Boger fluids prepared with PB1 as opposed to those prepared with PB2 (see Table 5). At the same time BF2 has a higher viscosity than that of BF1. While the sintering time t_{99} of BF2 is higher than that of BF1, the initial sintering rate is higher for BF1. Similar conclusions can be drawn for BF3 and BF4; i.e., BF3 coalesces faster than BF4 as indicated by t_{99} and confirmed by the initial sintering rate.

In order to examine the effect of elasticity on the sintering kinetics, it is necessary to compare the behavior of samples that have equivalent viscosities and interfacial tensions. In our samples, such a requirement is satisfied. In fact BF1 and BF2 are both characterized by small viscosities of roughly the same order of magnitude, and have similar interfacial tensions. BF3 and BF4 also have equivalent interfacial tensions when deposited on a PTFE substrate. The main difference is in their viscosity. Figure 12 shows that the model does not predict well the experimental data for BF4 and overestimates the sintering rate. The same behavior is seen for BF3.

As for PB2, the effect of the interfacial tension in relation with the viscosity was highlighted. One can thus conclude that the influence of the coupling between viscosity/interfacial tension is not a discriminating parameter between BF3 and BF4.

As demonstrated in Table 8, the reduced sintering times of BF1 and BF2 are different. The sintering time is of 2.76 for BF1 and 3.04 for BF2. These two fluids have the same interfacial tension and spreading parameter, but the main difference between them comes from their relaxation time, which is 0.6 s for BF1 and 0.9 s for BF2. They can even be compared with PB1; which has an interfacial tension similar to that of BF1 and BF2, but a lower relaxation time (10^{-5} s).

These results cannot be compared with those of PB2 because the effect of the viscosity coupled with the effect of the interfacial tension seems to play a greater part in the sintering process than for BF3 and BF4. This suggests that for samples having similar viscosity and similar interfacial tension, the relaxation time has an opposite effect. Samples with higher relaxation time exhibit a slower sintering process. This phenomenon is relatively well described by the theoretical mode that predicts a decrease in sintering rate with the relaxation time.

4. Concluding Remarks

The present paper presents an experimental study of the sintering process kinetics of two drops put in close vicinity on a solid substrate. Three model fluids were used: PDMS and PB with different viscosities and Boger fluids. The results showed that the rate of the sintering process is influenced by viscosity, interfacial tension, and elasticity. The viscosity and the elasticity of were found to oppose the coalescence, whereas the effect of surface tension was found to be more complex. It plays a major role beyond a certain critical viscosity, but below this viscosity threshold, the influence of the surface tension seems to be weak. Finally, the Bellehumeur et al. model was found to capture nicely the whole sintering process for Newtonian fluids and slightly overestimates the sintering rate for Boger fluids.

References and Notes

(1) Frenkel, J. *J. Phys.* **1945**, *9*, 385−391.
(2) Eshelby, J. D. (Discussion in paper by A. Shaler.) *Met. Trans.* **1949**, *185*, 806.
(3) Lontz, J. F. Study of Polymer Material. In *Fundamental Phenomena in the Material Science*; Bonis, L. J., Hausner, H. H., Eds.; Plenum Press: New York, 1964.
(4) Pokluda, O.; Bellehumeur, C. T.; Vlachopoulos, J. *AIChE J.* **1997**, *43*, 3253−3256.
(5) Bellehumeur, C. T.; Kontopoulou, M.; Vlachopoulos, J. *Rheol. Acta* **1998**, *37*, 270−278.
(6) Scribben, E.; Aaron, P. R.; Baird, G. D. *J. Rheol.* **2005**, *49*, 1159−1175.
(7) Scribben, E.; Baird, G. D.; Wappeon, P. *Rheol. Acta* **2006**, *45*, 825−839.
(8) Jagota, A.; Argento, C.; Mazur, S. *J. Appl. Phys.* **1998**, *83*, 250−259.
(9) Johnson, K. L.; Kendall, K.; Roberts, A. D. *Proc. R. Soc. London, Ser. A* **1971**, *324*, 301−313.
(10) Kendall, K.; Padget, J. C. *J. Adhes.* **1987**, *22*, 39−48.
(11) Hui, C. Y.; Baney, J. M.; Kramer, E. J. *Langmuir* **1998**, *14*, 6570−6578.
(12) Ross, J. W.; Miller, W. A.; Weatherly, G. C. *J. Appl. Phys.* **1981**, *52*, 3884−3888.
(13) Jagota, A.; Dawson, P. R. *Acta Metall.* **1988**, *36*, 2551−2561.
(14) Mazur, S.; Plazek, D. J. *Prog. Org. Coat.* **1994**, *24*, 225−236.
(15) Lin, Y. Y.; Hui, C. Y.; Jagota, A. *J. Colloid Interface Sci.* **2001**, *273*, 267−282.
(16) Perot, E.; Maazouz, A. *J. Polym. Eng.* **2007**, *27*, 267−289.
(17) Owens, D. K.; Wendt, R. C. *J. Appl. Polym. Sci.* **1969**, *13*, 1741−1747.

MA702349S